Approaches to structure and dynamics of biological systems by electron-paramagnetic-resonance spectroscopy

Scarpelli, F.

Chapter 5. The RIDME pulse sequence as an effective tool for measurements of electron-electron distances involving paramagnetic centers with strong spectral anisotropy

5.1 Introduction

Pulsed EPR has taken a leap forward as a method for structure determination in disordered chemical and biological systems ever since pulsed EPR methods had been developed that directly and selectively probe the dipolar interaction between electron spins [1-3]. Amongst them are 2+1 methods and DEER [4-6], solid-echo type single-frequency techniques for refocusing dipolar couplings (SIFTER) [7], and double quantum coherence methods (DQM) [5,6,8]. These techniques are optimized for systems with low spectral anisotropy, such as nitroxide-type spin labels and organic radicals, and require the excitation of a significant part of the spectrum. The spectral widths of the EPR transitions of nitroxides and organic radicals are in the order of several mT at the conventional operating frequency of 9 GHz (X-band EPR), which compares well with presently available excitation bandwidths of a few mT (e.g. a pulse length of 24 ns results in 1.5 mT bandwidth). For even the most benign transition metal ion, Cu(II), the spectral width is already about 70 mT. The resulting fractional excitation of the spectrum either severely limits the sensitivity or makes the application of the method impossible. Therefore, novel approaches to address such paramagnetic centers are sought. The present account describes a method tailored to determine the interaction between a low g-anisotropy center and a center of large g-anisotropy and is ideally suited to address the distance between a nitroxide spin label and a paramagnetic transition-metal ion. For structure determination this combination is

most relevant, because transition-metal centers are often present in proteins. Another advantage of such centers is that they are firmly anchored in the protein and therefore are not fraught with the problem of flexible linkers as the commonly used spin labels. Previously, most approaches to measure such distances made use of the change in relaxation properties of the small g-anisotropy center caused by the transition-metal ion, as discussed in several reviews [9-11]. The complexity of relaxation-based approaches from the point of view of experiment and interpretation has so far limited the applications.

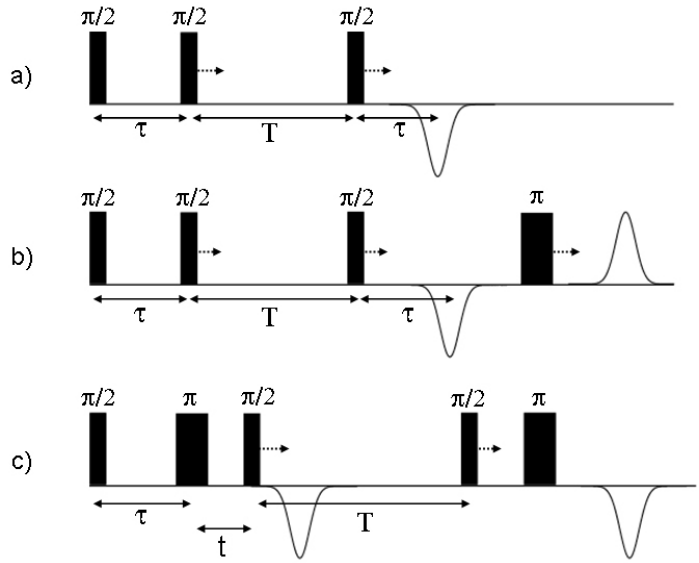

Fig. 1: Pulse sequences for RIDME experiment: (a) three-pulse RIDME and (b) four-pulse RIDME, time τ is incremented; (c) five-pulse RIDME, time t is incremented and echo is detected as a function of t- τ.

The method proposed directly probes the dipolar interaction between the metal center and the nitroxide. It is based on the relaxation induced dipolar modulation (RIDME) method suggested by Kulik et al [12], in which the change is detected in the resonance frequency of the observed

spin, i.e. the nitroxide (A-spins), by the spontaneous flip of the electron spin on the partner paramagnetic center (B-spins). Here the flip of the B-spins is not induced by a pump-pulse as in traditional sequences, but is left to the longitudinal relaxation of the B-spins. As a consequence, there is no need to flip the B-spins by a pump pulse, avoiding the problem of the limited excitation bandwidth. The RIDME sequence as proposed originally [12] (Fig. 1 a) and the four-pulse version suggested subsequently [13], suffer from a dead-time problem that severely limits the usefulness of these methods for distance determination involving systems with high g-anisotropy, as we will demonstrate.

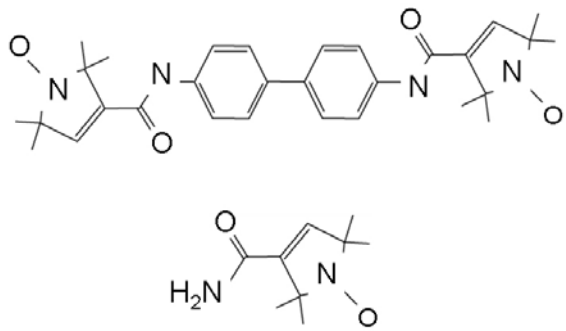

Fig. 2: Chemical structures of the biradical PH2 and the monoradical PH0

We propose a five-pulse version of the RIDME sequence that completely eliminates the dead-time. We demonstrate that the sequence works and that it yields the expected distances on a nitroxide biradical (PH2, see Fig. 2) by comparing the results of the new RIDME sequence and a conventional DEER experiment. Subsequently, we apply the new sequence to measure the distance between the low-spin iron(III) center, a paramagnetic center with large g-anisotropy, and a nitroxide spin label in cytochrome *f* (cyt *f*). This protein is part of the electron transfer chain in photosynthesis and contains an intrinsic low-spin Fe(III) center. By site-directed mutagenesis, a cystein was introduced and at position 104 and a spin label was attached. resulting in a system with a nitroxide-Fe(III) distance in the order of 1.43 nm. We show that in spite of the large g-

anisotropy of the Fe(III) center, the distance between the two paramagnetic centers can be determined. A Gaussian distance distribution centered at 1.67 nm with a width of 0.22 nm is obtained. Presently, there is no other method to determine distances in such cases with similar accuracy.

5.2 Materials and Methods

5.2.1 Sample preparation

The pEAF-wt [14] expression plasmid containing the sequence encoding the soluble domain of cyt *f* from *Nostoc* sp. PCC7119 has been kindly provided by the group of Prof. Miguel De la Rosa, Instituto de Bioquímica Vegetal y Fotosíntesis, Universidad de Sevilla, Spain. In order to prepare the single-cysteine Cyt *f* variants Q104C and N71C, mutations were introduced by site-directed mutagenesis using the Quik Change™ polymerase chain reaction protocol (Stragene, La Jolla, CA) with the plasmid pEAF-wt as a template. To introduce a cysteine instead of the asparagines at the position 71 the direct primer GGCTC***C***AAGGTCGGCTTA***TG***CGTCGGTGCTG (31 bases) was designed from the nucleotide sequence, inserting at the same time the Sty I restriction site next to the *5'* end of the leader of this primer. Analogously, to introduce a cysteine instead of the glutamine at the position 104 the direct primer CGGCGATGTTTACTTC***TGC***CCCTACGGCGAAG (32 bases) was designed, inserting an extra Bgl I restriction site with respect to the *wild type*. Both constructs were verified by DNA sequencing.
To improve the maturation and correct insertion of the heme group, *E. coli* strain MV1190 cells (Bio-Rad) were co-transformed with plasmids pEC86 [14] and the Cyt *f* expression plasmids. The cells were incubated on Luria-Bertani (LB) medium plates (added by 20 mg/L ampicillin, 20 mg/L chloramphenicol) at 37º C for 24 hours. Several pre-cultures were incubated in 100 mL flasks with 20 mL of LB medium supplemented with 20 mg/L ampicillin (amp) and 20 mg/L chloramphenicol (cam) at 37º C and 250 rpm for 5-6 hours. The pre-cultures with the best OD_{600} were used to inoculate 1.7 L (in 5 L Erlenmeyer flasks) in the same medium and incubated at 25º C and 150 rpm for >72 h under semi-

anaerobic conditions and high antibiotics pressure by adding further amp and cam after 20 h and 40 h. Induction was achieved 20 h after the inoculation of the large culture using 1mM IPTG. More than 80 h from the induction the cultures appeared brown for the presence of the cyt; the cells were harvested by centrifugation and the periplasmic fraction was extracted by osmotic shock. The pink water fraction was dialyzed against 2 L of 5 mM Tris-HCl buffer, pH 8 and 3 mM dithiothreitol (DDT). The yield in the periplasmatic fraction was 10 mg/L of protein for N71C and 5 mg/L of Q104C. The resulting dialysate was cleared by centrifugation and loaded onto a DEAE column equilibrated with 5 mM Tris-HCl buffer, pH 8 and 3 mM DDT. Elution has been performed with a gradient of 20–500 mM NaCl and 3 mM DTT. The fractions containing the cyt *f* were concentrated and loaded onto a gel-filtration (G75 Superdex) column and eluted with 5 mM Tris-HCl buffer pH 8, 3mM DTT and 150 mM NaCl. The fractions containing the protein were pooled, concentrated, dialysed against 5 mM Mes pH 6 and 3 mM DTT and loaded onto a DEAE column equilibrate with 5 mM Mes pH 6 and 3 mM DTT. The protein was eluted with a gradient 0-500 mM NaCl and tested for its purity using the A_{280}/A_{556} ratio. The pure fractions show an A_{280}/A_{556} value of 1.3 under reducing conditions.
Before adding the spin label the excess of DTT has been removed from the purified cyt *f* cysteine mutant solution, by several concentration/redilution cycles with degassed 10 mM Na phosphate at pH 6. To avoid reduction of the disulfide by the Fe(II) and concomitant loss of the spin label, a 100 fold excess of $K_3[Fe(CN)_6]$ was added to the solution before adding a 10 fold excess of MTSL [(1-Oxyl-2,2,5,5,-tetramethyl-3-pyrroline-3-m3thyl)-methanethiosulfonate] (purchased from Toronto Research Chemicals, Ont., Canada). The solution was left for 2h at room temperature and overnight at 4º C; the excess of $K_3[Fe(CN)_6]$ and MTSL was removed by several concentration/redilution cycles with degassed 10 mM Na phosphate at pH 6.

5.2.2 EPR experiments

All measurements were done on a Bruker E680 ElexSys spectrometer equipped with an ER 4118X-MS3 split-ring resonator of the FlexLine series and an Oxford cryostat. Initial pulse positions for five-pulse RIDME sequence were 0, 500 ns, 960 ns, *T*+960 ns, *T*+X (for *T* values

see text below), X was 2000 ns for nitroxide biradical and 1800 ns for spin labeled cyt *f*. Detector integration gate was 20 ns. Positions of the third and the fourth pulses were incremented with a step of 4 ns, while positions of the other pulses as well as the detection gate were not changed.

All experiments on nitroxide solutions were done at 40K with a repetition time of 10 ms. Pulse lengths for the RIDME experiments were 24 ns and 48 ns for $\frac{\pi}{2}$- and π-pulses, respectively, to compromise between broad excitation bandwidth required to cover spectrally dipolar doublets and sufficiently narrow bandwidth needed to escape simultaneous excitation of both spins in the radical couple. All RIDME measurements were done at magnetic field value of 332.75 mT and microwave frequency of 9.372 GHz.

DEER measurements were done using 9.332 GHz observer frequency with initial observer pulse positions 0, 500 ns, 1400 ns. Pump pulse of frequency 9.397 GHz was initially positioned at 400 ns and swept with a step of 4 ns. The RIDME traces of PH2 are obtained by dividing a trace with T = 400 μs by one with T = 10 μs. The value of the external magnetic field for DEER was 331.3 mT.

All experiments were done at 7 K with a repetition time of approximately 1 s and 2 shots per loop. Applied pulse lengths of 12 ns and 24 ns for $\frac{\pi}{2}$- and π-pulses respectively were shortest achievable on our spectrometer. The RIDME traces of both systems (Q104C and N71C) were obtained by dividing a trace with T = 200 μs by one with T = 5 μs. The microwave frequency and magnetic field value were 9.306 GHz and 330.45 mT respectively.

5.2.3 Numerical calculation

All numerical calculations were done using the R2006b version of the MATLAB software. To calculate Pake distributions and the corresponding dipolar traces, we assumed the orientation distributions for the g-tensor and the inter-radical vector to be isotropic and mutually independent. To avoid numerical singularities for the Pake distributions, we assumed an intrinsic Gaussian line width of 1 MHz.

5.3 Results and Discussion

In the following we first describe the background relevant to the method and introduce the new pulse sequence. Then we report measurements of the nitroxide-nitroxide distance in PH2 and of the distance between a nitroxide spin label and the low-spin Fe(III)-center in the cyt *f* mutant.

5.3.1 Background of the method, dipolar interaction between two electron spins

The dipole-dipole interaction between two unpaired electrons is described by the Hamiltonian [15]

$$H_{dd} = \frac{1}{r^3}\left[\left(\vec{\mu}_1 \cdot \vec{\mu}_2\right) - 3\frac{\left(\vec{\mu}_1 \cdot \vec{r}\right)\left(\vec{\mu}_2 \cdot \vec{r}\right)}{r^2}\right]$$

For two interacting S=1/2 spins in the point-dipole approximation, the strength of the interaction in frequency units is given by

$$\omega_{dd} = \frac{\mu_0 g_1 g_2 \beta_e^2}{4\pi \mathrm{h}} \frac{1}{r^3}\left(3\cos^2\theta - 1\right)$$

Here g_1 and g_2 are the g values of the two interacting spins, r is the distance between them, and θ is the angle between the external magnetic field and the vector connecting the radicals. Typically, for organic radicals such as nitroxides, the g anisotropy is very small and one simply assumes $g_1 = g_2 = g_e = 2$. In this case, from the angular dependence of ω_{dd} a Pake pattern results [16] with two symmetric sharp peaks at

$$\omega_{dd}^{\perp} = \pm\frac{\mu_0 \beta_e^2}{\pi \hbar}\frac{1}{r^3}$$

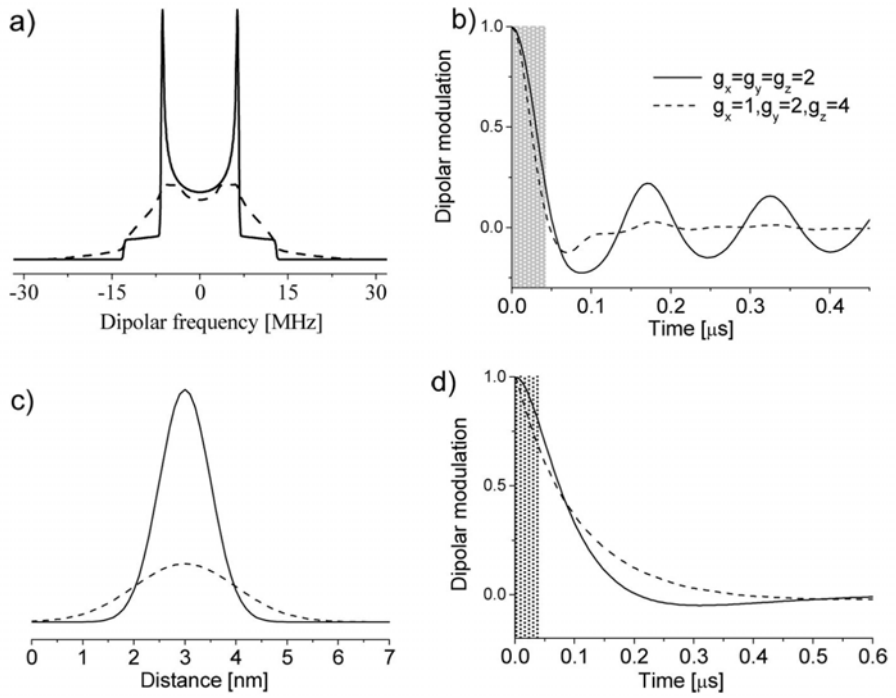

Fig. 3: (a) Pake patterns for isotropic g-tensor: solid line, and for rhombic g-tensor with $g_x = 1$ $g_y = 2$ $g_z = 4$: dashed line; (b) Corresponding dipolar modulations; (c) two Gaussian distance distribution functions with corresponding dipolar traces in case of g-tensor anisotropy with $g_x = 1$ $g_y = 2$ $g_z = 4$. Shadowed bars on figures (b) and (d) indicate the dead time areas of the four-pulse RIDME sequence.

The numerically calculated Pake pattern for an inter-radical distance of 2 nm is shown in Fig. 3 a (solid line). It has two sharp peaks at $\upsilon_{dd}^{\perp} = \pm$ 6.3 MHz. In the time domain, a slowly decaying modulation of the dipolar trace results (solid line, Fig.3 b). For the coupling between an isotropic spin with g = 2 and a spin with a large g anisotropy (principal values: $g_x = 1, g_y = 2, g_z = 4$), the dashed line in Fig. 3 a is obtained The larger g anisotropy causes a broadening of the Pake pattern. In the

time domain (Fig. 3 b, dashed line) the initial part of the modulation up until approx. 60 ns is similar to the isotropic case, but all subsequent modulations are absent.

5.3.2 The standard RIDME sequence

The pulse sequence for the RIDME experiment is the stimulated echo sequence shown in Fig. 1 a. A full analytical description of the method is given in [12]. Here we illustrate the idea of the method with a vector model. The initial magnetization vector in the rotating frame is $\{0,0,-M_0\}$. After the first $\frac{\pi}{2}$-pulse, which as all following pulses is applied along the x-axis, the magnetization becomes $\{0,-M_0,0\}$. After a time τ of free evolution the vector is given by $\{-M_0 \sin\Omega\tau,-M_0 \cos\Omega\tau,0\}$, where Ω is the off-resonance frequency of the spin packet. The second $\frac{\pi}{2}$-pulse transforms the magnetization vector into $\{-M_0 \sin\Omega\tau,0,M_0 \cos\Omega\tau\}$. Under free evolution for a time T that is much larger than the transverse relaxation time T_2, only the z-component survives, resulting in $\{0,0,M_0 \cos\Omega\tau\}$. The immediate result of the third $\frac{\pi}{2}$-pulse is the magnetization vector $\{0,M_0 \cos\Omega\tau,0\}$, which can be presented as the sum of two vectors: $\left\{-\frac{M_0}{2}\sin\Omega\tau,\frac{M_0}{2}\cos\Omega\tau,0\right\}$ and $\left\{\frac{M_0}{2}\sin\Omega\tau,\frac{M_0}{2}\cos\Omega\tau,0\right\}$. The first vector is refocused after a time τ of free evolution resulting in a stimulated echo. The second vector continues defocusing, but it can be refocused by the application of an additional π-pulse resulting in a virtual echo [17]. If during the time T a B-spin, i.e. a spin that has a dipolar interaction with the observed A-spin, flips, the frequency of the A-spin shifts by ω_{dd}, resulting in a modulation of the amplitude for both the stimulated and the virtual echo. By incrementing the time τ in the sequence, this is detected as a cosine function of $\omega_{dd}\tau$. The probability of the flip of the B-spins during the time T is given by

$$\frac{1}{2}\left(1-\exp\left\{-\frac{T}{T_1}\right\}\right) \tag{1}$$

where T_1 is the longitudinal relaxation time of the B-spin. Consequently, T has to be in the order of T_1 and the modulation depth, given by (1), is maximally 0.5 of the echo amplitude.
This simple three-pulse RIDME sequence, however, suffers from the dead time problem, i.e., τ cannot be made infinitely small. The experimental inaccessibility of the short τ values, in this case, has two origins. First, resonator ringing prevents echo detection immediately after the third pulse. Second, at τ values comparable with the pulse widths, partial or complete overlap of the first and the second pulse causes distortions of the RIDME trace in exactly the same way as in the basic, three-pulse version of the DEER sequence. The previously proposed four-pulse modification of RIDME with an additional refocusing π-pulse, as shown on Fig.1 b, removes the resonator ringing problem, and reduces the dead time to about 40 ns [13]. Still, the remaining dead time seriously limits the application of the RIDME method to systems where at least one of the coupled spins has a large spectral anisotropy, as discussed in the following.

5.3.3 Consequences of the dead time for systems with large g-anisotropy

In Fig. 3 b, the effect of a large g-anisotropy on the time trace is shown. Whereas for systems with small g-anisotropy the information about the distance between the coupled spins can be obtained even without taking into account the initial part of the trace, for systems with large g-anisotropy the shape of the function (Fig. 3 b, dashed line) cannot be reconstructed without measuring the initial part of the trace. This part of the trace is lost in the shaded area that shows the minimal dead time achievable by the traditional RIDME sequences. Fig. 3 c and d show the effect of a distribution of distances and the time domain data (Fig. 3 d). Distinct time domain traces are obtained, from which the distance distributions can be reconstructed provided that the full trace can be determined experimentally.

5.3.4 Pulse sequence for dead-time free, five-pulse RIDME

In order to remove the residual dead time an additional π-pulse is introduced into the four-pulse RIDME sequence [12] using a similar approach as was done to develop the four-pulse DEER sequence [18]. The resulting five-pulse RIDME sequence is shown in Fig. 1 c. For the detection, one can use either the refocused stimulated or the refocused virtual echo, since both of them are modulated in the same way. In our hands, detection on the refocused virtual echo worked best. The amplitude of this echo is measured as a function of the time delay between the third pulse and the primary echo created by the first two pulses. The positions of the third and the fourth pulse are simultaneously incremented by the same time steps, keeping the time T between them constant. The positions of the first, second and the fifth pulse are kept fixed in time. The total phase-evolution time is constant, avoiding unwanted contributions of T_2 relaxation to the trace.

Although the dead time is eliminated in the same way as in the DEER experiment there is one difference to be considered. At *t* values close to zero, three echoes, namely the refocused stimulated, the refocused virtual and the echo created by the last two pulses of the sequence overlap in time. This distorts the trace at initial times. To remove this problem, phase cycling is required. We use the 8-step phase cycle outlined in table 1. According to the vector model, the amplitudes of the three echoes depend on the phases of the third (φ_3) and fourth (φ_4) pulse. The refocused virtual echo depends on $e^{i(\varphi_4-\varphi_3)}$, the refocused stimulated echo on $e^{i(\varphi_3+\varphi_4)}$ and the two-pulse echo of the last two pulses in the sequence on $e^{i\varphi_4}$. In principle, the phase cycle $\left[(+x)+(-x)+(+y)+(-y)\right]$ on the third and the fourth pulse would be sufficient to eliminate the unwanted echoes. However, if the time T is long, the two refocused echoes can be much smaller in amplitude than the primary echo. In this case, imperfections in the microwave-channel phase adjustment may prevent complete cancellation of the unwanted two-pulse echo. Therefore, an additional two-step phase cycle$\left[(+x)-(-x)\right]$is applied to the first pulse, to remove remaining distortions from the time trace.

Table 1
Phase cycle used for the 5 pulse RIDME sequence

φ_1	φ_3	φ_4	Detection
+x	+x	+x	+
+x	-x	-x	+
+x	+y	+y	+
+x	-y	-y	+
-x	+x	+x	-
-x	-x	-x	-
-x	+y	+y	-
-x	-y	-y	-

5.3.5 Suppression of unwanted contribution to the RIDME trace

Additionally to the dipolar modulations, nuclear modulations and spectral diffusion can contribute to the RIDME traces at temperatures below 70 K. The latter two contributions can be eliminated most reliably by dividing the measured trace by a reference trace of a sample containing only A spins. But even if such a sample is not available, the unwanted contributions can be largely suppressed. As was shown before [19], nuclear modulations can be suppressed by dividing two traces, one with sufficiently long T, where dipolar contribution is substantial, and the other with a much shorter T (T_S) that is still long compared with T_2. In that case, the nuclear modulations should be similar to those in the first trace thus removing the major part of the nuclear modulations. In other words, terms independent of T would cancel each other and terms depending on T would decay owing to the loss of nuclear coherence. This procedure, however, does not remove the second unwanted contribution, the spectral diffusion in the time interval T. Spectral diffusion causes a monotonous decay of the RIDME trace, even though the total echo-refocusing path remains the same. The best experimental conditions for separation of the spectral diffusion component from the dipolar modulations would be to find a parameter T long enough to flip a large fraction of the partner spins but still short enough to avoid spectral diffusion. In practice, at least for the experiments discussed

here, spectral diffusion components are sufficiently distinct from dipolar modulations that they can be empirically fitted and subtracted.

5.3.6 Results for the nitroxide biradical

To test the new pulse sequence we used the nitroxide biradical PH2 (Fig. 2), because in this system the distance is well-defined and regular DEER experiments can be performed to verify the RIDME results. In Fig. 4 b, the DEER result is shown, revealing the regular modulation pattern in the time trace. For RIDME, the system is not ideal, because the paramagnetic centers, and in particular their T_1 times, are identical. This is not desired, since significant modulation depths can only be obtained if the time T of the RIDME sequence is comparable to or longer than T_1 of the B-spins. Here, however, the A-spins have the same T_1, making it impossible to detect their signal after such a long T time. Nevertheless, RIDME traces can be obtained as shown in Fig. 4 c, solid line. Owing to the small modulation depth for RIDME, nuclear modulations of protons appear alongside the desired electron-electron dipolar modulations. To eliminate the nuclear modulations, the RIDME trace for the PH0 monoradical (dashed line on Fig.4 c) was measured, revealing only nuclear-modulation and spectral-diffusion components. Division of the trace for PH2 by the one for PH0 results in the trace shown in Fig. 4 d, in which nuclear modulations and the overall decay of the trace, which is due to spectral diffusion, are absent. The trace is in agreement with the DEER trace, Fig. 4 b, showing that the RIDME modulations obtained with the new sequence are indeed caused by the electron-electron spin interaction. The modulation depth is in the order of 15 %, i.e., significantly lower than the theoretical maximum of 50 %. Given that T is 400 μs and that the T_1 of nitroxides at this temperature is in the ms range, the conditions are far from ideal for efficient RIDME (Eq. 1), which explains the low modulation depth. The dashed line in Fig. 4 d shows the fit of the dipolar trace using DeerAnalysis2006 [20-22] with a Gaussian distance distribution at 1.89 nm and 0.14 nm standard deviation. Faithful reproduction of the experimental curves including the early times confirms that the new RIDME sequence abolishes the dead time and results in the proper shape of the early parts of the curve. The DEER trace, obtained with the same pulse lengths for the observer

pulses as the RIDME trace (Fig. 4 b) was fitted with parameters of 1.89 nm, and a standard deviation of 0.08 nm. We attribute the smaller width of the distribution in the latter case to orientation selection in that combination of pump and observer pulses.

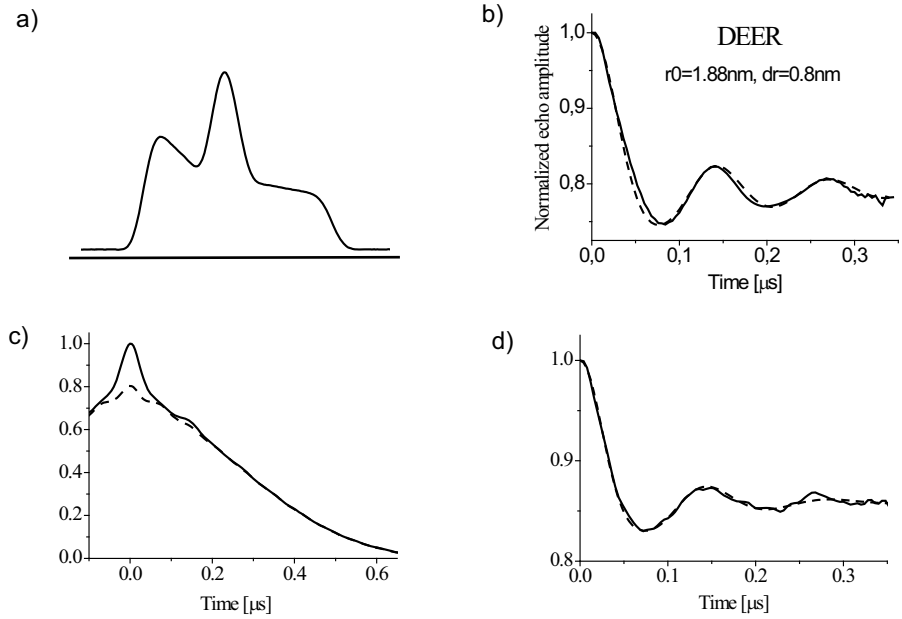

Fig. 4: Experimental data obtained for PH2 biradical. (a) Two-pulse echo detected spectrum with two arrows indicating observer spins excited in both DEER and RIDME; (b) DEER trace: solid line and best fit: dashed line; (c) five pulse RIDME trace for PH2 biradical: solid line, for PH0 monoradical: dashed line, obtained as described in text; (d) extracted from RIDME traces dipolar modulations: solid line, and its best fit: dashed line.

5.3.7 Results for spin labelled Cytochrome *f*

The new pulse sequence has been developed for the correlation of a transition metal ion and a spin label, which we demonstrate for the

protein cyt *f* (Q104C), where the spin label interacts with a low-spin Fe(III) center. The RIDME trace for Q104C is shown in Fig. 5 a. At times longer than 70 ns, the trace is dominated by the background, which is fitted as a stretched exponential (see Fig. 5 a) and subtracted (Fig. 5 b). A fast initial decay is observed, but further modulations, as seen in the traces in Fig. 4 b at times larger than 100 ns, are absent. The dotted line in Fig. 5 b shows the fit to the data with low-spin Fe(III) g-values of $g_x = 0.9$, $g_y = 1.69$, $g_z = 3.51$ [23], and a Gaussian distance distribution centered at 1.67 nm with a standard deviation of 0.22 nm. The parameters of the distance distribution are only marginally affected by the uncertainty of the g_x value, resulting in variations of about 0.04 nm in the distance and the width for g_x = 0.4, 0.9 or 1.4.
In Fig. 5 c, the dependence of the modulation depth on T is shown. For data obtained by dividing a trace with a long T by one with a short T (T_S) (see above) the dependence can be described by a bi-exponential curve according to

$$A = A_0\left[P\left(e^{-\frac{T_S}{T_1^a}} - e^{-\frac{T}{T_1^a}}\right) + (1-P)\left(e^{-\frac{T_S}{T_1^b}} - e^{-\frac{T}{T_1^b}}\right)\right] \qquad (2)$$

In the present case, T_S = 5 µs, and T_1^a and T_1^b are the relaxation times of the fast relaxing center. The fraction P refers to the amount of spins relaxing with a time T_1^a and A_0 is the modulation depth obtained for an optimal choice of T and T_S. For T_1^a and T_1^b we obtained 13 µs and 148 µs, respectively, which is in good agreement with the values for low-spin iron hemes at this temperature [24]. We attribute the presence of two T_1 times with approximately equal weight (P = 0.57) to the anisotropy of the low-spin Fe(III) relaxation times. There is no literature about the anisotropy of T_1 of the low-spin Fe(III), nevertheless a similar anisotropy of T_1 has been found for nitroxide-radical centers [25]. Also, preliminary measurements on a second mutant (cyt *f* N71C) yielded similar parameters in eq. 2, emphasizing that the low-spin Fe(III) center is the source of the modulation. The amplitude A_0 = 0.24 for Q104C is about half the maximal modulation depth for RIDME, which, according

to eq. 1 is 0.5. The smaller depth found agrees with the fraction of oxidized iron in our samples, which is 56% as determined by optical spectroscopy. Taking this correction into account we conclude that A_0 is 86% of the theoretical maximum. This high value also shows that possible distortions due to limited bandwidth of the microwave pulses for such short distances are not significant.

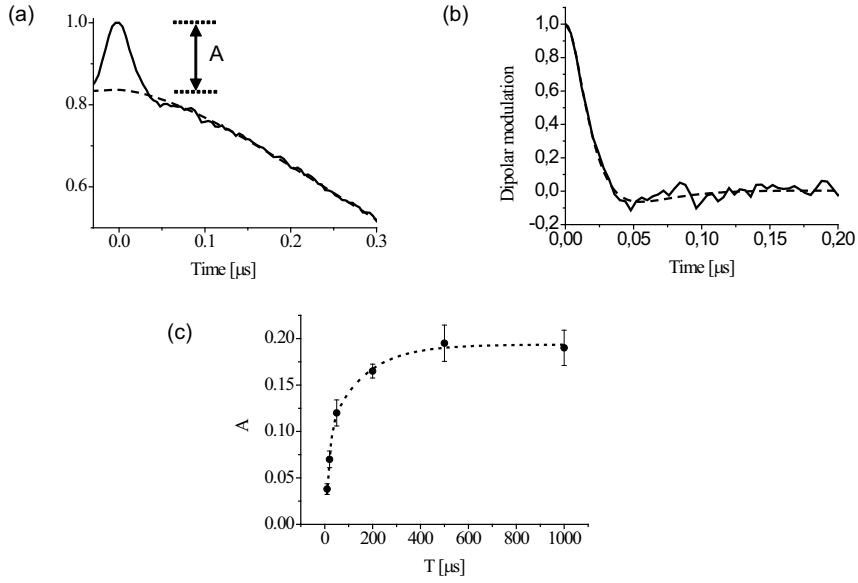

Fig. 5: Results for Q104 mutant of Cytochrome *f*. (a) Experimental five-pulse RIDME trace (solid line) obtained as described in the text and stretched exponential fit of the background (dashed line); (b) extracted dipolar modulation contribution (solid line) and its best fit (dashed line); (c) Modulation amplitude defined as shown on (a) versus time T (points) and the best fit (dashed line)

In Table 2, the parameters of the distance distribution are compared to the distance between the iron and the C_β atoms (Fe- C_β) derived from the X-ray structure of cyt *f*. Given the length of 0.5 - 0.6 nm [8] for the spin-label linker, between the C_β-atom and the center of spin density on the nitroxide, the distance found for Q104C agrees well with the C_β distance

obtained from the crystallography. Additionally, the conformation of the spin-label linker was modeled [26,27], resulting in the distance distribution shown in Fig. 6.
The model collects all sterically allowed orientations of the spin label and neglects any attractive interactions between protein and spin label. Therefore model-derived distributions are expected to be broader than the real ones. Taking this into account, the distance distribution found by RIDME is in good agreement with the distance of the paramagnetic centers predicted from the model.

Table 2
Distance for cyt *f* mutant Q104 and crystal structure parameters

sample	**distance** nm	σ_r	**C-beta Fe** nm[a]
Q104C	1.67±0.03	0.22±0.08	1.43

[a]From X-ray crystallography, structure PDB-entry 1TU2

The width of the distance distribution of Q104C is 0.22 nm, which is smaller than the distance distributions found for the distances between two spin labels linked to a single protein (between 0.24 and 0.45 nm [27]). This is reasonable in view of the fact that the distribution is dominated by the spread in spin-label linker conformations and that in the present case only one such distribution is to be considered. An odd dichotomy arises. The distance determined between a spin label and a metal center should be more accurate because only one spin-label linker conformation affects the distance distribution. On the other hand the g-tensor anisotropy of the metal center abolishes the later time part of the modulation making it more difficult to extract distances and their distributions. Nevertheless, reliable distance information can be extracted, provided that a dead-time free method is used.

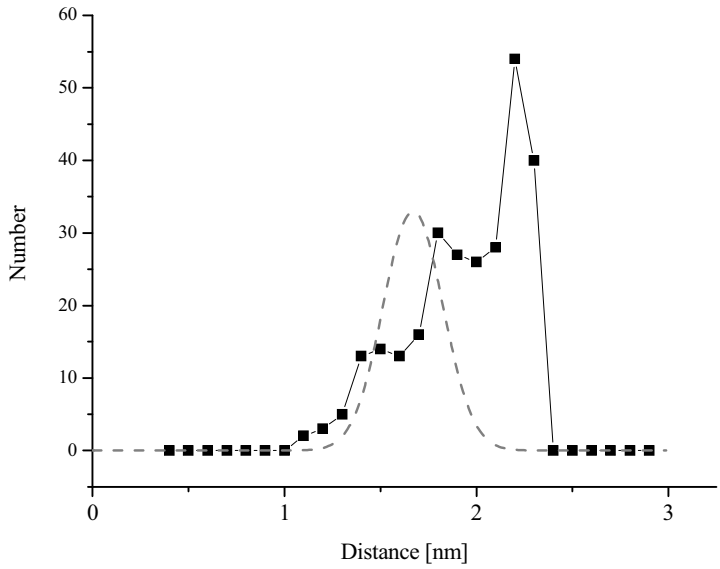

Fig. 6: Distance distribution of Q104C mutant (dashed) superimposed on distance distribution from the model to describe the spin label conformations (see text)

5.4 Conclusion

We demonstrate why for a reliable measurement of distances and distance distributions between transition-metal centers and radicals dead-time free dipolar modulation traces are required. Therefore, the dead-time free version of the RIDME method, as introduced here, will significantly enhance the existing sequence. Limitations of relaxation times and excitation bandwidths define the distance ranges accessible, which, similar to the DEER method should range from 1.5 nm to about 5 nm. Exclusive sensitivity to dipolar interaction makes the method selective to the distances of interest.

Acknowledgments

I would like to thank dr. Sergey Milikisyants who developed the 5-pulse RIDME sequence and the analysis program and Michela Finiguerra for the preparation of the cytochrome *f* samples.

Reference list

1. Schiemann, O.; Prisner, T. F. *Quarterly Reviews of Biophysics* **2007,** *40* (1), 1-53.
2. Borbat, P. P.; Freed, J. H. *Two-Component Signaling Systems, Pt B* **2007,** *423*, 52-62.
3. Jeschke, G.; Polyhach, Y. *Physical Chemistry Chemical Physics* **2007,** *9* (16), 1895-1910.
4. Milov, A. D.; Salikhov, K. M.; Shchirov, M. D. *Sov. Phys. Solid State (Fizika Tverdogo Tela)* **1981,** *23*, 565-569.
5. Saxena, S.; Freed, J. H. *Chemical Physics Letters* **1996,** *251* (1-2), 102-110.
6. Saxena, S.; Freed, J. H. *Journal Of Chemical Physics* **1997,** *107* (5), 1317-1340.
7. Jeschke, G.; Pannier, M.; Godt, A.; Spiess, H. W. *Chemical Physics Letters* **2000,** *331* (2-4), 243-252.
8. Borbat, P. P.; Freed, J. H. *Chemical Physics Letters* **1999,** *313* (1-2), 145-154.
9. Berliner, L. J.; Eaton, S. S.; Eaton, G. R. *Distance Measurements in Biological Systems by EPR;* Kluver Academic/Plenum Publishers: New York, 2000; Vol. 19.
10. Eaton, S. S.; Eaton, G. R. *Structures and Mechanisms: from Ashes to Enzymes* **2002,** *827*, 321-339.
11. Eaton, S. S.; Eaton, G. R. *Coordination Chemistry Reviews* **1988,** *83*, 29-72.
12. Kulik, L. V.; Dzuba, S. A.; Grigoryev, I. A.; Tsvetkov, Y. D. *Chemical Physics Letters* **2001,** *343* (3-4), 315-324.
13. Kulik, L. V.; Grishin, Y. A.; Dzuba, S. A.; Grigoryev, I. A.; Klyatskaya, S. V.; Vasilevsky, S. F.; Tsvetkov, Y. D. *Journal of Magnetic Resonance* **2002,** *157* (1), 61-68.
14. Albarran, C.; Navarro, J. A.; Molina-Heredia, F. P.; Murdoch, P. S.; De la Rosa, M. A.; Hervas, M. *Biochemistry* **2005,** *44* (34), 11601-11607.
15. Abragam, A.; Bleaney, B. I. *Electron paramagnetic resonance of transition ions;* 1970.
16. Pake, G. E. *Journal of Chemical Physics* **1948,** *16* (4), 327-336.
17. Bloom, A. L. *Physical Review* **1955,** *98* (4), 1105-1111.
18. Pannier, M.; Veit, S.; Godt, A.; Jeschke, G.; Spiess, H. W. *Journal of Magnetic Resonance* **2000,** *142* (2), 331-340.

19. Savitsky, A.; Dubinskii, A. A.; Flores, M.; Lubitz, W.; Mobius, K. *Journal of Physical Chemistry B* **2007,** *111* (22), 6245-6262.
20. Jeschke, G.; Koch, A.; Jonas, U.; Godt, A. *Journal Of Magnetic Resonance* **2002,** *155* (1), 72-82.
21. Jeschke, G.; Chechik, V.; Ionita, P.; Godt, A.; Zimmermann, H.; Banham, J.; Timmel, C. R.; Hilger, D.; Jung, H. *Appl. Magn. Reson.* **2006,** *30* (3-4), 473-498.
22. Jeschke, G. *Macromolecular Rapid Communications* **2002,** *23* (4), 227-246.
23. Schunemann, V.; Trautwein, A. X.; Illerhaus, J.; Haehnel, W. *Biochemistry* **1999,** *38* (28), 8981-8991.
24. Zhou, Y.; Bowler, B. E.; Eaton, G. R.; Eaton, S. S. *Journal of Magnetic Resonance* **1999,** *139* (1), 165-174.
25. Du, J. L.; Eaton, G. R.; Eaton, S. S. *Journal of magnetic resonance, Series A* **1994,** *115*, 213-221.
26. Volkov, A. N.; Worrall, J. A. R.; Holtzmann, E.; Ubbink, M. *Proceedings Of The National Academy Of Sciences Of The United States Of America* **2006,** *103* (50), 18945-18950.
27. Finiguerra, M. G.; Prudencio, M.; Ubbink, M.; Huber, M. *Magnetic Resonance In Chemistry* **2008,** in press.